Detection and extraction of fault surfaces in 3-D seismic data

Israel Cohen, Technion - Israel Institute of Technology, Nicholas Coult, Augsburg College, and Anthony A. Vassiliou, GeoEnergy*

Summary

In this paper, an efficient method is proposed for detecting and extracting fault surfaces in 3-D seismic volumes. The seismic data is transformed into a volume of *local fault extraction* (LFE) estimates, representing the likelihood that a given point lies on a fault surface. The fault surfaces are partitioned into relatively small linear portions, which are identified by analyzing tilted and rotated subvolumes throughout the region of interest. Directional filtering and thresholding further enhance the seismic discontinuities attributable to fault surfaces.

Introduction

Seismic interpretation can be broadly subdivided into two components: structural, which investigates the nature and geometry of the subsurface structures; and stratigraphic, which investigate the subsurface stratigraphy. A major component of the structural interpretation is the identification, location and extraction of individual fault surfaces. Fault surfaces are common subterranean structures, associated with displacements or offsets of seismic layers. Their consistent and reliable detection in 3-D seismic data provides an interpreter with very powerful means to quickly visualize and map complex geological structures. A common tool facilitating structural and stratigraphic interpretation is the coherency cube, originated by Bahorich and Farmer (Bahorich and Farmer, 1995). It is calculated from the seismic data using a coherency measure that quantifies the seismic discontinuity at each point. Discontinuities attributable to fault surfaces include dip, azimuth, and offset changes of seismic reflectors, and waveform and amplitude variations caused by defocusing. Such discontinuities appear on coherence slices as incoherent linear or curved features (Marfurt et al., 1999; Gersztenkorn and Marfurt, 1999; Neff et al., 2000; Lees, 1999).

The most acceptable coherence measures are based on cross-correlation (Bahorich and Farmer, 1995), semblance (Marfurt et al., 1998), or eigenstructure (Gersztenkorn and Marfurt, 1999; Gersztenkorn et al., 1999; Kirlin, 1992) techniques. These methods typically suffer from either a lack of robustness, especially when dealing with noisy data, or high computational complexity (Marfurt et al., 1999; Gersztenkorn and Marfurt, 1999). Recently, a robust and computationally efficient analysis method was introduced for the estimation of seismic coherency (Cohen and Coifman, 2002). It involves a coherency measure, namely the *local structural entropy* (LSE), which evaluates the dissimilarity of subvolumes enclosing a given analysis point. Dealing with subvolumes, rather than individual traces, leads to robustness, while avoiding the expensive computations of semblance and eigenstructure-based large covariance matrices and eigenvalues. A major drawback of coherency-based fault analysis is that seismic discontinuities may also result from geological features, which are unrelated to faults. Furthermore, creating a consistent geological interpretation from large 3-D seismic data volumes often requires manual intervention, which is time-consuming, tedious and imprecise.

In this paper, which summarizes the results in (Cohen et al., 2005), we propose a robust and computationally efficient method for the extraction of fault surfaces in 3-D seismic volumes. The seismic data is transformed into a volume of *local fault extraction* (LFE) estimates, which provides the interpreter with a much clearer visual indication of the fault surfaces. The LFE estimate at a given analysis point is obtained by the following procedure. First, a 3-D analysis cube, tilted and rotated about the analysis point, is selected by the interpreter. The analysis cube moves throughout the seismic volume and outputs for each point a measure of *normalized differential entropy* (NDE). The NDE value represents the likelihood of a fault surface, having similar dip and azimuth as of the analysis cube, to intersect with the analysis point. Subsequently, the local average of the NDE is removed, and portions of fault surfaces, approximately aligned with the analysis cube, are extracted by directional filtering. The filtered NDE coefficients are thresholded, and filtered back to produce directional LFE volumes. Finally, the LFE attribute is given by the maximal directional LFE, over the presumably tested set of dips and azimuths. This practically gathers the significant portions of the fault surfaces into smooth larger surfaces.

Local Fault Extraction

In this section we describe the basic components forming the proposed fault extraction algorithm.

Normalized Differential Entropy

We begin by subtracting the mean value from each trace of the seismic data . Specifically, the data is modified by

$$\hat{d}_{xyt} = d_{xyt} - E_t\left\{d_{xyt}\right\} = d_{xyt} - \tfrac{1}{N_t}\sum_{k=1}^{N_t} d_{xyk}\,, \qquad (1)$$

where d_{xyt} and $\hat{d}_{xyt}$ are respectively the original and modified t-th sample of the trace at position (x, y), and N_t is the total number of samples in each trace. Then, a relatively small 3-D analysis cube is selected by the in-

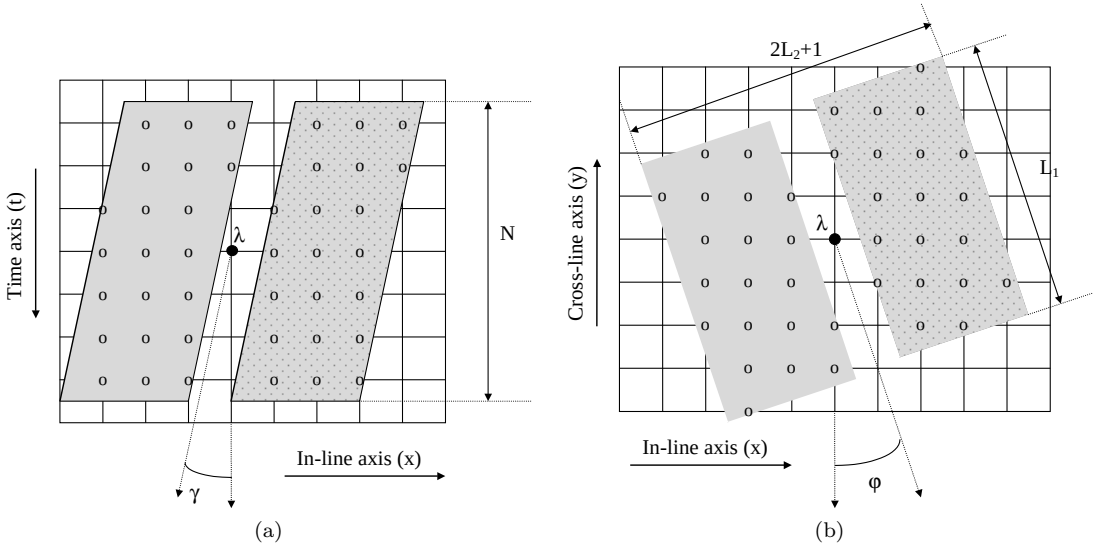

Fig. 1: (a) A vertical cross-section and (b) horizontal slice illustrating the geometrical distribution of traces and samples used in the analysis cube. The analysis cube, consisting of two subvolumes, is centered about an analysis point $\lambda = (x, y, t)$, and defined by length of major axis L_1, length of minor axis $2L_2 + 1$, time duration N samples, azimuth φ, and dip γ.

terpreter. The analysis cube moves throughout the 3-D modified seismic volume and outputs for each point a measure of NDE.

The analysis cube is defined by the length of major axis L_1, length of minor axis $2L_2 + 1$, time duration N samples, azimuth φ, and dip γ (Fig. 1). It comprises two identical subvolumes, which are tilted and rotated about the analysis point $\lambda = (x, y, t)$. The samples within the two subvolumes are rearranged in a consistent manner into two column vectors $\mathbf{v}_{1,\lambda}(\gamma, \varphi)$ and $\mathbf{v}_{2,\lambda}(\gamma, \varphi)$. The NDE at the analysis point λ is defined by the normalized difference of this two vectors:

$$\mathcal{N}_\lambda(\gamma, \varphi) = \frac{\|\mathbf{v}_{1,\lambda}(\gamma, \varphi) - \mathbf{v}_{2,\lambda}(\gamma, \varphi)\|_p}{\|\mathbf{v}_{1,\lambda}(\gamma, \varphi)\|_p + \|\mathbf{v}_{2,\lambda}(\gamma, \varphi)\|_p}\,, \qquad (2)$$

where $\|\cdot\|_p$ is the ℓ_p norm. The NDE is a gradient based formula and is a normalized version of the Prewitt edge detection filter (Jain, 1989). It provides an extension of edge detection to surface detection in three dimensions. Specifically, if the two subvolumes are perfectly correlated without a disruption or offset of seismic layers, presumably there is no fault surface enclosed between them, so $\mathbf{v}_{1,\lambda}(\gamma, \varphi) = \mathbf{v}_{2,\lambda}(\gamma, \varphi)$ and $\mathcal{N}_\lambda(\gamma, \varphi) = 0$. Otherwise, the likelihood for the presence of a fault surface, aligned in the gap between the two subvolumes, is proportional to the offset of $\mathbf{v}_{1,\lambda}(\gamma, \varphi)$ and $\mathbf{v}_{2,\lambda}(\gamma, \varphi)$. In this case, $0 < \mathcal{N}_\lambda(\gamma, \varphi) \leq 1$, where the maximum value of $\mathcal{N}_\lambda(\gamma, \varphi)$ is obtained for maximally offset correlated subvolumes, *i.e.*, $\mathbf{v}_{1,\lambda}(\gamma, \varphi) = -\mathbf{v}_{2,\lambda}(\gamma, \varphi)$.

Contrast Enhancement

The second step of the algorithm is contrast enhancement. Fault surfaces having dips and azimuths about the same dip and azimuth of the analysis cube are distinguished by higher NDE values, compared to the local average NDE value. Accordingly, we apply a contrast enhancement filtering to the NDE values, and set to zero negative values. This facilitates the analysis of regions that contain dipping layers or are highly discontinuous.

The contrast enhancement filtering can be efficiently implemented using a discrete "Mexican Hat" function:

$$f(n) = C(1 - n^2)\exp(-n^2/2) \qquad (3)$$

where $n = k\tau$ ($k \in \mathbb{Z}$), and C is a normalization constant such that $\sum_{k=-\infty}^{\infty} |f(k\tau)| = 2$. We use a finite length filter ($-4.5 \leq n \leq 4.5$), containing odd number of uniformly spaced coefficients (we obtained good results for 31 coefficients, but generally it depends on the size of the analysis cube and the "thickness" of the fault surfaces). The filtered NDE is given by:

$$\bar{\mathcal{N}}_\lambda(\gamma, \varphi) = g_\lambda(\gamma, \varphi) * \mathcal{N}_\lambda(\gamma, \varphi) = \sum_{\lambda'} g_{\lambda-\lambda'}(\gamma, \varphi)\mathcal{N}_{\lambda'}(\gamma, \varphi)\,, \qquad (4)$$

where $g_\lambda(\gamma, \varphi)$ is a rotated version of f, such that its main axis is perpendicular to the slabs of the analysis cube. The contrast enhanced NDE is given by

$$\hat{\mathcal{N}}_\lambda(\gamma, \varphi) = \max\left\{\bar{\mathcal{N}}_\lambda(\gamma, \varphi),\, 0\right\}\,. \qquad (5)$$

Directional LFE

The third step of the algorithm is directional filtering. In this step, we extract the portions of fault surfaces that are approximately aligned with the analysis cube.

The directional filter, denoted by $h_\lambda(\gamma+\alpha,\varphi)$, is a 3-D ellipsoid, tilted by $\gamma+\alpha$ with respect to the time axis, rotated by φ with respect to the in-line axis, and normalized by $\sum_\lambda h_\lambda(\gamma,\varphi)=1$. Its dimensions, selected by the interpreter, control the minimal dimensions of the detected subsurfaces. The maximum value of α is determined by the dip increment Δ_γ ($|\alpha|<\Delta_\gamma/2$). In our implementation, we used a 3-D pencil-like shaped Hanning window, whose dimensions are 61 samples at its major axis and 3 samples at its minor axes. The dip increment is $\Delta_\gamma=5^o$, and the relative tilt of the directional filter α is restricted to $\{-2^o,0,2^o\}$. Clearly, we could use a smaller dip increment and discard the relative tilt. However, the above formulation is computationally more efficient.

Directional filtering of the contrast enhanced NDE yields

$$C_\lambda(\gamma+\alpha,\varphi)=\sum_{\lambda'}h_{\lambda-\lambda'}(\gamma+\alpha,\varphi)\hat{\mathcal{N}}_{\lambda'}(\gamma,\varphi)\,. \qquad (6)$$

These coefficients are thresholded by δ ($0<\delta<1$),

$$\tilde{C}_{\lambda'}(\gamma+\alpha,\varphi)=\begin{cases}C_{\lambda'}(\gamma+\alpha,\varphi), & \text{if } C_{\lambda'}(\gamma+\alpha,\varphi)\geq\delta\\ 0, & \text{otherwise,}\end{cases} \qquad (7)$$

and then filtered back to produce the directional LFE, given by

$$\mathcal{L}_\lambda(\gamma,\varphi)=\sum_{\lambda',\alpha}\tilde{C}_{\lambda'}(\gamma+\alpha,\varphi)h_{\lambda-\lambda'}(\gamma+\alpha,\varphi)\,. \qquad (8)$$

The directional LFE volumes contain significant portions of fault surfaces, characterized by roughly the same dip and azimuth orientations as those of the analysis cube.

Constructing the Fault Surfaces

The final step of the algorithm is keeping at each point the maximum directional LFE value, over the tested set of dips and azimuths. Specifically, the LFE attribute at the analysis point λ is given by

$$\mathcal{L}_\lambda=\max_{\gamma,\varphi}\{\mathcal{L}_\lambda(\gamma,\varphi)\}\,. \qquad (9)$$

The LFE volume thus gathers and connects the significant portions of faults into smooth large fault surfaces.

Results

In this section we use a real data example to demonstrate the applicability of the LFE algorithm, and to illustrate its execution. The data example (courtesy of GeoEnergy) is from the Gulf of Mexico. The data is decimated in both time and space. The time interval is $8\,ms$, in-line trace spacing is $25\,m$, and cross-line trace spacing is $50\,m$. A small subvolume with an in-line distance of $5.025\,km$ and a cross-line distance of $10.05\,km$ (201 x 201 traces) is used for demonstration. Each trace is $3.208\,s$ in duration (401 samples).

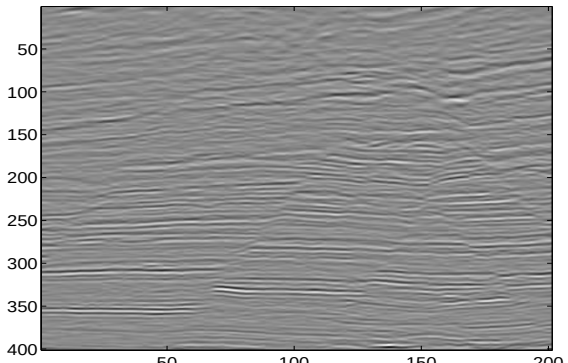

Fig. 2: A vertical cross-section through the seismic data at $y=6\,km$.

Fig. 2 shows a vertical cross-section through the seismic data at $y=6\,km$. Cross-sections through the NDE and directional LFE volumes, corresponding to an analysis cube of [7 7 21] samples with dip $\gamma=-20^o$ and azimuth $\varphi=0^o$, are displayed in Fig. 3. Clearly, the dip and azimuth of the analysis cube determine the portions of fault surfaces to be detected. In particular, surfaces having dips and azimuths about the same dip and azimuth of the analysis cube are distinguished by higher NDE values, compared to the locally averaged NDE. The second step of the algorithm is contrast enhancement. This step removes the 3-D local average of the NDE, thus compensating for regions that are highly discontinuous, but often do not contain fault surfaces. The third step of the algorithm is directional filtering. Here, we detect the portions of fault surfaces that are approximately aligned with the analysis cube. The minimal dimensions of the detected subsurfaces are controlled by the dimensions of the directional filter. For the present example, we used a 3-D pencil-like shaped Hanning filter, whose dimensions are 61 samples at its major axis and 3 samples at its minor axes. The dip increment is $\Delta_\gamma=5^o$, the azimuth increment is $\Delta_\varphi=45^o$, and the relative tilt of the directional filter α is restricted to $\{-2^o,0,2^o\}$. The filtered NDE coefficients are thresholded by $\delta=0.12$, and filtered back to produce the directional LFE volumes. The result of the third step of the algorithm, for -20^o dip and 0^o azimuth, is shown in Fig. 3(b). The final step is keeping at each point the maximum directional LFE value, over the tested set of dips and azimuths. This yields the LFE volume (Fig. 4), containing all the fault surfaces in conformity with the presumed model (*i.e.*, the dimensions of the analysis cube, set of dips and azimuths, directional filter, threshold, *etc.*).

Conclusion

Recently, there has been progress in visualizing stratigraphic and structural discontinuities with the coherence methods, which look at the similarity of a small number of neighboring traces to determine discontinuities. However the efficiency of existing coherence methods for extracting fault surfaces is inadequate. The proposed

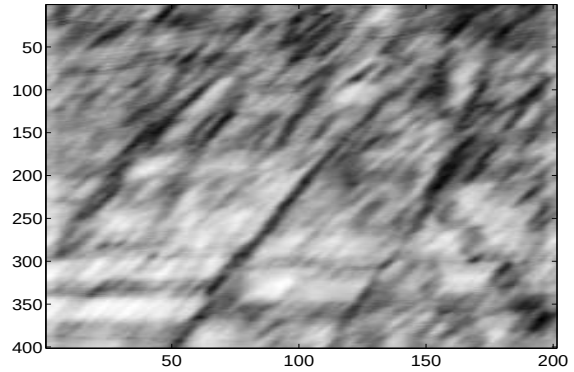

(a)

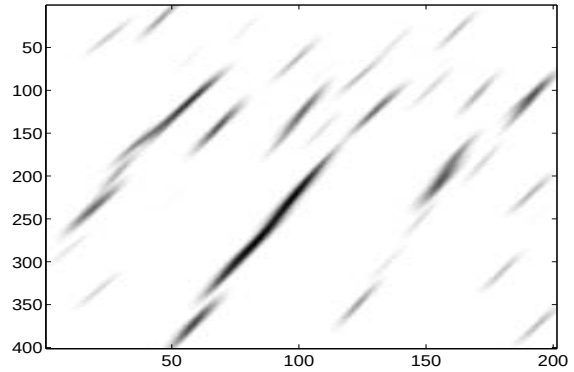

(b)

Fig. 3: Vertical cross-sections at $y = 6\,km$ through (a) the Normalized Differential Entropy volume, and (b) the directional LFE volume, using an analysis cube of [7 7 21] samples with dip $\gamma = -20^o$ and azimuth $\varphi = 0^o$.

algorithm facilitates the extraction of the fault surfaces, by identifying portions of the surfaces and combining them into large fault surfaces. Specifically, the portions of the fault surfaces are identified by analyzing tilted and rotated subvolumes throughout the region of interest, and subsequently 3-D contrast enhancement and directional filtering. Moreover, equipped with the dip and azimuth arguments which yield maximum in (9), the LFE method can be further enhanced by 3-D skeletonisation and 3-D surface separation. The ultimate result of the fault extraction computations are well defined, cleanly separated, labelled fault surfaces, which can be readily used for seismic interpretation.

References

Bahorich, M. S., and Farmer, S. L., 1995, 3-d seismic discontinuity for faults and stratigraphic features: The Leading Edge, **14**, 1053–1058.

Cohen, I., and Coifman, R. R., 2002, Local discontinuity measures for 3-d seismic data: Geophysics, **67**, 1933–1945.

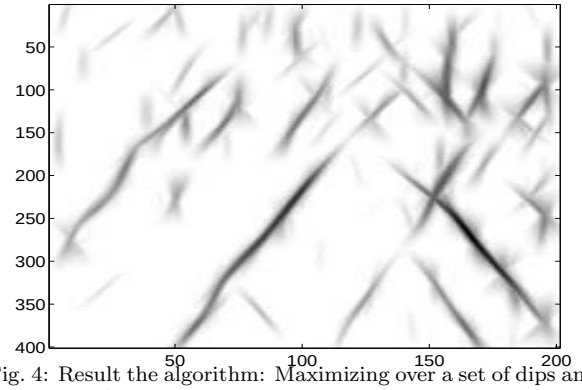

Fig. 4: Result the algorithm: Maximizing over a set of dips and azimuths. A vertical cross-section at $y = 6\,km$ through the LFE volume, using an analysis cube of [7 7 21] samples, dips $\gamma = -20^o, -15^o, \ldots, 20^o$, and azimuths $\varphi = -45^o, 0^o, 45^o, 90^o$.

Cohen, I., Coult, N., and Vassiliou, A. A., 2005, Detection and extraction of fault surfaces in 3-d seismic data: submitted to Geophysics.

Gersztenkorn, A., and Marfurt, K. J., 1999, Eigenstructure-based coherence computations as an aid to 3-d structural and stratigraphic mapping: Geophysics, **64**, 1468–1479.

Gersztenkorn, A., Sharp, J., and Marfurt, K. J., 1999, Delineation of tectonic features offshore trinidad using 3-d seismic coherence: The Leading Edge, **18**, 1000–1008.

Jain, A. K., 1989, Fundamentals of digital image processing: Prentice Hall.

Kirlin, R. L., 1992, The relationship between semblance and eigenstructure velocity estimators: Geophysics, **57**, 1027–1033.

Lees, J. A., 1999, Constructing faults from seed picks by voxel tracking: The Leading Edge, pages 338–340.

Marfurt, K. J., Kirlin, R. L., Farmer, S. L., and Bahorich, M. S., 1998, 3-d seismic attributes using a semblance-based coherency algorithm: Geophysics, **63**, 1150–1165.

Marfurt, K. J., Sudhaker, V., Gersztenkorn, A., Crawford, K. D., and Nissen, S. E., 1999, Coherency calculations in the presence of structural dip: Geophysics, **64**, 104–111.

Neff, D. B., Grismore, J. R., and Lucas, W. A., Automated seismic fault detection and picking:, US Patent 6 018 498, 2000.

Acknowledgements

The authors thank Prof. Ronald R. Coifman of Yale University for valuable discussions and helpful suggestions.